arXiv:1701.03979v1 [cond-mat.quant-gas] 15 Jan 2017

Analytical coupled-channels treatment of two-body scattering in the presence of three-dimensional isotropic spin-orbit coupling

Q. Guan[1] and D. Blume[1]

[1]*Department of Physics and Astronomy, Washington State University, Pullman, Washington 99164-2814, USA*

(Dated: January 17, 2017)

It is shown that the single-particle spin-orbit coupling terms, which—in the cold atom context—are associated with synthetic gauge fields, can significantly and non-trivially modify the phase accumulation at small interparticle distances even if the length scale $(k_{\rm so})^{-1}$ associated with the spin-orbit coupling term is significantly larger than the van der Waals length $r_{\rm vdW}$ that characterizes the two-body interaction potential. A theoretical framework, which utilizes a generalized local frame transformation and accounts for the phase accumulation analytically, is developed. Comparison with numerical coupled-channels calculations demonstrates that the phase accumulation can, to a very good approximation, be described over a wide range of energies by the free-space scattering phase shifts—evaluated at a scattering energy that depends on $k_{\rm so}$—and the spin-orbit coupling strength $k_{\rm so}$.

PACS numbers:

The tunability of low-energy scattering parameters such as the s-wave scattering length a_s and p-wave scattering volume V_p by means of application of an external magnetic field in the vicinity of a Feshbach resonance [1] has transformed the field of ultracold atom physics, providing experimentalists with a knob to "dial in" the desired Hamiltonian. This tunability has afforded the investigation of a host of new phenomena including the BEC-BCS crossover [2, 3]. Most theoretical treatments of these phenomena are formulated in terms of a few scattering quantities such as a_s and V_p, which properly describe the low-energy behavior of the two-body system.

The recent realization of spin-orbit coupled cold atom systems [4] is considered another milestone, opening the door for the observation of topological properties and providing a new platform with which to study scenarios typically encountered in condensed matter systems with unprecedented control [5–7]. An assumption that underlies most theoretical treatments of cold atom systems with synthetic gauge fields is that the spin-orbit coupling term, i.e., the Raman laser that couples the different internal states or the shaking of the lattice that couples different bands, leaves the atom-atom interactions "untouched". More specifically, mean-field treatments "simply" add the single-particle spin-orbit coupling term to the mean-field Hamiltonian and parameterize the atom-atom interactions via contact potentials with coupling strengths that are calculated for the two-body van der Waals potential without the spin-orbit coupling terms [7, 8].

Consistent with such mean-field approaches, most two-body scattering studies derive observables based on the assumption that the two-body Bethe-Peierls boundary condition, derived in the absence of single-particle spin-orbit coupling terms, remains unaffected by the spin-orbit coupling terms, provided an appropriate "basis transformation" is accounted for [9–16]. The underlying premise of these two-body and mean-field treatments is rooted in scale separation, which suggests that the free-space scattering length a_s and scattering volume V_p remain good quantities provided $(k_{\rm so})^{-1}$ is larger than the two-body van der Waals length $r_{\rm vdW}$. Indeed, model calculations for a square-well potential in the presence of three-dimensional isotropic spin-orbit coupling suggest that the above reasoning holds, provided $1/a_s$ and V_p are small [17].

This work revisits the question of how to obtain and parameterize two-body scattering observables in the presence of three-dimensional isotropic spin-orbit coupling. Contrary to what has been reported in the literature, our calculations for Lennard-Jones and square-well potentials show that the three-dimensional isotropic spin-orbit coupling terms can impact the phase accumulation in the small interparticle distance region where the two-body interaction potential cannot be neglected even if $(k_{\rm so})^{-1}$ is notably larger than $r_{\rm vdW}$. We observe non-perturbative changes of the scattering observables when $k_{\rm so}$ changes by a small amount. An analytical treatment, which reproduces the full coupled-channels results such as the energy-dependent two-body cross sections for the finite-range potentials with high accuracy, is developed. Our analytical treatment relies, as do previous treatments [9–13, 15–17], on separating the short- and large-distance regions. The short-distance Hamiltonian is treated by applying a gauge transformation, followed by a rotation, that "replaces" the $\mathbf{p}$-dependent spin-orbit coupling term by an $\mathbf{r}$- and $\mathbf{p}$-independent diagonal matrix ($\mathbf{r}$ and $\mathbf{p}$ denote the relative position and momentum vectors, respectively). The diagonal terms, which can be interpreted as shifting the scattering energy in each channel, can introduce non-perturbative changes in the scattering observables for small changes in $k_{\rm so}$, especially when V_p is large. We note that our derivation of the short-distance Hamiltonian, although similar in spirit, differs in subtle but important ways from what is presented in Ref. [10, 12].

Our analytical framework also paves the way for designing energy-dependent zero-range or δ-shell pseudo-

potentials applicable to systems with spin-orbit coupling. While energy-dependent pseudo-potentials have proven useful in describing systems without spin-orbit coupling [18, 19], generalizations to systems with spin-orbit coupling are non-trivial due to the more intricate nature of the dispersion curves. Our results suggest a paradigm shift in thinking about spin-orbit coupled systems with non-vanishing two-body interactions. While the usual approach is to assume that the short-distance behavior or the effective coupling strengths are not impacted by the spin-orbit coupling terms, our results suggest that they can be for specific parameter combinations. Even though our analysis is carried out for the case of three-dimensional isotropic spin-orbit coupling, our results point toward a more general conclusion, namely that spin-orbit coupling terms may, in general, notably modify the phase accumulation in the short-distance region.

We consider two particles with position vectors $\mathbf{r}_j$ and masses m_j ($j = 1$ and 2) interacting through a spherically symmetric two-body potential $V_{\rm int}(r)$ ($r = |\mathbf{r}_1 - \mathbf{r}_2|$). Both particles feel the isotropic spin-orbit coupling term with strength $k_{\rm so}$, $V_{\rm so}^{(j)} = \hbar k_{\rm so} \mathbf{p}_j \cdot \boldsymbol{\sigma}^{(j)}/m_j$, where $\mathbf{p}_j$ denotes the canonical momentum operator of the jth particle and $\boldsymbol{\sigma}^{(j)}$ the vector that contains the three Pauli matrices $\boldsymbol{\sigma}_x^{(j)}$, $\boldsymbol{\sigma}_y^{(j)}$ and $\boldsymbol{\sigma}_z^{(j)}$ for the jth particle. Throughout, we assume that the expectation value of the total momentum operator $\mathbf{P}$ of the two-body system vanishes. In this case, the total angular momentum operator $\mathbf{J}$, $\mathbf{J} = \mathbf{l} + \mathbf{S}$, of the two-particle system commutes with the system Hamiltonian and the scattering solutions can be labeled by the quantum numbers J and M_J; M_J denotes the projection quantum number, $\mathbf{l}$ is the relative orbital angular momentum operator, and $\mathbf{S} = \hbar(\boldsymbol{\sigma}^{(1)} + \boldsymbol{\sigma}^{(2)})/2$.

Separating off the center of mass degrees of freedom, the relative Hamiltonian H for the reduced mass μ particle with relative momentum operator $\mathbf{p}$ can be written as a sum of the free-space Hamiltonian $H_{\rm fs}$ and the spin-orbit coupling term $V_{\rm so}$, $H = H_{\rm fs} + V_{\rm so}$, where

$$H_{\rm fs} = \left[\frac{\mathbf{p}^2}{2\mu} + V_{\rm int}(r)\right] I_1 \otimes I_2 \tag{1}$$

and $V_{so} = \hbar k_{so} \boldsymbol{\Sigma} \cdot \mathbf{p}/\mu$ with $\boldsymbol{\Sigma} = (m_2 \boldsymbol{\sigma}^{(1)} \otimes I_2 - m_1 I_1 \otimes \boldsymbol{\sigma}^{(2)})/M$. Here, I_j denotes the 2×2 identity matrix that spans the spin degrees of freedom of the jth particle and M the total mass, $M = m_1 + m_2$. For each (J, M_J) channel, the $\mathbf{r}$-dependent eigen functions $\Psi^{(J,M_J)}$ are expanded as [13, 15, 16]

$$\Psi^{(J,M_J)}(\mathbf{r}) = \sum_{l,S} r^{-1} u_{l,S}^{(J)}(k, r) |J, M_J; l, S\rangle, \tag{2}$$

where the sum goes over $(l, S) = (0, 0)$ and $(1, 1)$ for $(J, M_J) = (0, 0)$ and over $(l, S) = (J, 0)$, $(J, 1)$, $(J-1, 1)$, and $(J+1, 1)$ for $J > 0$. In the $|J, M_J; l, S\rangle$ basis (using the order of the states just given), the scaled radial set of differential equations for fixed J and M_J reads $\underline{h}^{(J)} \underline{u}^{(J)} = E \underline{u}^{(J)}$, where $\underline{h}^{(J)}$ [20] denotes the scaled radial Hamiltonian for a given J (note that the Hamiltonian is independent of the M_J quantum number). For $r > r_{\rm max}$, the interaction potential $V_{\rm int}$ can be neglected and $\underline{u}^{(J)}$ is matched to the analytic asymptotic $V_{\rm int} = 0$ solution [13, 15, 16]

$$\underline{u}^{(J)} \xrightarrow[r > r_{\rm max}]{} r \left(\underline{\mathcal{J}}^{(J)} - \underline{\mathcal{N}}^{(J)} \underline{K}^{(J)}\right), \tag{3}$$

where $\underline{\mathcal{J}}^{(J)}$ and $\underline{\mathcal{N}}^{(J)}$ are matrices that contain the regular and irregular solutions for finite $k_{\rm so}$ (for $J = 0$ and 1, explicit expressions are given in Ref. [16]). Defining the logarithmic derivative matrix $\underline{\mathcal{L}}^{(J)}(r)$ through $(\underline{u}^{(J)})'(\underline{u}^{(J)})^{-1}$, where the prime denotes the partial derivative with respect to r, the K-matrix is given by

$$\underline{K}^{(J)} = \left[\left(r\underline{\mathcal{N}}^{(J)}\right)' - \underline{\mathcal{L}}^{(J)}(r)\left(r\underline{\mathcal{N}}^{(J)}\right)'\right] \times \left[\left(r\underline{\mathcal{J}}^{(J)}\right)' - \underline{\mathcal{L}}^{(J)}(r)\left(r\underline{\mathcal{J}}^{(J)}\right)\right]\Big|_{r=r_{\rm max}}, \tag{4}$$

the S-matrix by $\underline{S}^{(J)} = (\underline{I} + \imath \underline{K}^{(J)})(\underline{I} - \imath \underline{K}^{(J)})^{-1}$, where $\underline{I}$ denotes the identity matrix, and the cross sections by $\sigma_{\alpha\beta} = 2\pi |\underline{S}_{\beta\alpha}^{(J)} - \delta_{\alpha\beta}|^2/k_\alpha^2$, where α and β each take the values $1, 2, \cdots$.

In general, the K-matrix has to be determined numerically via coupled-channels calculations. In what follows, we address the question whether $\underline{K}$ can, at least approximately, be described in terms of the logarithmic derivative matrix of the free-space Hamiltonian $H_{\rm fs}$. If the spin-orbit coupling term $V_{\rm so}$ vanished in the small r limit, one could straightforwardly apply a projection or frame transformation approach [21–24] that would project the inner small r solution, calculated assuming that $V_{\rm so}$ vanishes in the inner region, onto the outer large r solution, calculated assuming that $V_{\rm int}$ vanishes in the outer region [25]. The fact that $V_{\rm so}$ does not vanish in the small r limit requires, as we show below, a generalization of the frame transformation approach.

We start with the Hamiltonian H and define a new Hamiltonian $\tilde{H}$ through $T^{-1}HT$, where T is an operator to be determined. The solution $\tilde{\Psi}$ of the new Hamiltonian is related to the solution Ψ of H through $\tilde{\Psi} = T^{-1}\Psi$; here and in what follows we drop the superscripts "(J, M_J)" and "(J)" for notational convenience. The operator T reads RU, where $R = \exp(-\imath k_{\rm so} \boldsymbol{\Sigma} \cdot \mathbf{r})$; the form of U is introduced later. To calculate $H_R = R^{-1} H R$, we use

$$R^{-1} H_{\rm fs} R = H_{\rm fs} - V_{\rm so} - E_{\rm so} \left[\boldsymbol{\Sigma} \cdot \mathbf{r}, \boldsymbol{\Sigma} \cdot \nabla\right] + \mathcal{O}(\mathbf{r}) \tag{5}$$

and

$$R^{-1} V_{\rm so} R = V_{\rm so} + 2 \left[\boldsymbol{\Sigma} \cdot \mathbf{r}, \boldsymbol{\Sigma} \cdot \nabla\right] + \mathcal{O}(\mathbf{r}), \tag{6}$$

where $-\imath\hbar\nabla = \mathbf{p}$ and $E_{\rm so} = \hbar^2 k_{\rm so}^2/(2\mu)$ and where the notation $\mathcal{O}(\mathbf{r})$ indicates that terms of order r and higher are neglected ($\mathbf{r}$ "counts" as being of order r and $\mathbf{p}$ as being of order r^{-1}). Adding Eqs. (5) and (6) and neglecting the $\mathcal{O}(\mathbf{r})$ terms, we find that the spin-orbit coupling

term $V_{\rm so}$ is replaced by a commutator that arises from the fact that the operator $\mathbf{\Sigma}\cdot\mathbf{p}$ does not commute with the exponent of R,

$$H_R^{\rm sr} = H_{\rm fs} + E_{\rm so}\left[\mathbf{\Sigma}\cdot\mathbf{r}, \mathbf{\Sigma}\cdot\nabla\right]. \tag{7}$$

Here, the superscript "sr" indicates that this Hamiltonian is only valid for small r.

Our goal is now to evaluate the second term on the right hand side of Eq. (7). Defining the scaled short-distance Hamiltonian $h_R^{\rm sr}$ through $rH_R^{\rm sr}r^{-1}$ and expressing $h_R^{\rm sr}$ in the $|J, M_J; l, S\rangle$ basis, we find

$$\underline{h}_R^{\rm sr} = \left(\frac{-\hbar^2}{2\mu}\frac{\partial^2}{\partial r^2} + V_{\rm int}(r)\right) I_1\otimes I_2 + \underline{\mathcal{V}} + \underline{\epsilon}, \tag{8}$$

where $\underline{\mathcal{V}}$ is a diagonal matrix with diagonal elements $\hbar^2 l(l+1)/(2\mu r^2)$. For $J=0$, the matrix $\underline{\epsilon}$ is diagonal with diagonal elements $-3E_{\rm so}$ and $E_{\rm so}$. For $J>0$, in contrast, the 11 and 22 elements are, in general, coupled:

$$\underline{\epsilon} = E_{\rm so}\begin{pmatrix} -3 & c/M^2 & 0 & 0 \\ c/M^2 & -(\Delta M/M)^2 & 0 & 0 \\ 0 & 0 & d_1/M^2 & 0 \\ 0 & 0 & 0 & d_2/M^2 \end{pmatrix}, \tag{9}$$

where $\Delta M = m_1 - m_2$, $c = 2\sqrt{J(J+1)}(m_2^2 - m_1^2)$, $d_1 = -JM^2 - (J+1)\Delta M^2$, and $d_2 = 4m_1m_2 - d_1$. Since the r-dependent 11 and 22 elements of $\underline{\mathcal{V}}$ are identical (recall $l = J$ for these two elements), the matrix $\underline{U}$, which is defined such that $\underline{U}^{-1}\underline{\epsilon}\underline{U}$ is diagonal, also diagonalizes $\underline{h}_R^{\rm sr}$, i.e., the short-range Hamiltonian $\underline{\tilde{h}}_T^{\rm sr} = \underline{U}^{-1}\underline{h}_R^{\rm sr}\underline{U}$ is diagonal. This implies that the scaled radial short-distance Schrödinger equation $\underline{\tilde{h}}_T^{\rm sr}\underline{v} = E\underline{v}$ can be solved using standard propagation schemes such as the Johnson algorithm [26]. This Schrödinger equation differs from the "normal" free-space Schrödinger equation by channel-specific energy shifts. These shifts introduce a non-trivial modification of the phase accumulation in the short-distance region and—if a zero-range or δ-shell pseudo-potential description was used—of the boundary condition. While the energy shifts do, in many cases, have a negligible effect, our analysis below shows that they can introduce non-perturbative corrections in experimentally relevant parameter regimes. The channel-specific energy shifts are not taken into account in Ref. [12].

To relate the logarithmic derivative matrix $\underline{\tilde{\mathcal{L}}}^{\rm sr}(r) = \underline{v}'\underline{v}^{-1}$ of the scaled short-distance Hamiltonian $\underline{\tilde{h}}_T^{\rm sr}$ to the logarithmic derivative matrix $\underline{\mathcal{L}}(r)$, the "$T$-operation" needs to be "undone". Assuming that the short-distance Hamiltonian provides a faithful description, i.e., assuming that the higher-order correction terms can, indeed, be neglected for $r < r_{\rm max}$, we obtain

$$\underline{\mathcal{L}}(r_{\rm max}) \approx \left\{\underline{T}\underline{\tilde{\mathcal{L}}}^{\rm sr}(r)\underline{T}^{-1} - \underline{T}\left(\underline{T}^{-1}\right)'\right\}\Big|_{r=r_{\rm max}}. \tag{10}$$

To illustrate the results, we focus on the $J=0$ subspace. Denoting the usual free-space phase shifts at scattering energy $\hbar^2k^2/(2\mu)$ for the interaction potential $V_{\rm int}$ for the s-wave and p-wave channels by $\delta_s(k)$ and $\delta_p(k)$, respectively, the short-range K-matrix $\underline{\tilde{K}}^{\rm sr}$ for the Hamiltonian $\underline{\tilde{h}}_T^{\rm sr}$ has the diagonal elements $\tan(\delta_s(k_s))$ and $\tan(\delta_p(k_p))$, where $\hbar^2k_s^2/(2\mu) = E + 3E_{\rm so}$ and $\hbar^2k_p^2/(2\mu) = E - E_{\rm so}$. If we now, motivated by the concept of scale separation, make the assumption that the phase shifts $\tan(\delta_s(k_s))$ and $\tan(\delta_p(k_p))$ are accumulated at $r=0$ and correspondingly take the $r_{\rm max}\to 0$ limit of Eq. (4) with $\underline{\mathcal{L}}^{(J)}$ given by the right hand side of Eq. (10), we obtain the following zero-range K-matrix,

$$\underline{K}^{\rm zr} = -\frac{a_s(k_s)}{k_+ - k_-}\begin{bmatrix} k_+^2 & k_+k_- \\ k_+k_- & k_-^2 \end{bmatrix} - \frac{V_p(k_p)}{k_+ - k_-}\begin{bmatrix} k_+^2(k_- - k_{\rm so})^2 & k_+k_-(k_+ - k_{\rm so})(k_- - k_{\rm so}) \\ k_+k_-(k_+ - k_{\rm so})(k_- - k_{\rm so}) & k_-^2(k_+ - k_{\rm so})^2 \end{bmatrix}, \tag{11}$$

where $\hbar k_\pm = \pm\sqrt{2\mu(E+E_{\rm so})} - \hbar k_{\rm so}$.

To validate our analytical results, we perform numerical coupled-channels calculations. Since the wave function in the $J=0$ subspace is anti-symmetric under the simultaneous exchange of the spatial and spin degrees of freedom of the two particles, the solutions apply to two identical fermions. The Schrödinger equation for the Lennard-Jones potential $V_{\rm LJ}(r) = C_{12}/r^{12} - C_6/r^6$, with C_6 and C_{12} denoting positive coefficients, is solved numerically [27]. The solid lines in Figs. 1 and 2 show the partial cross section σ_{22} and the K-matrix element K_{22} as a function of $k_{\rm so}$ for vanishing scattering energy E for a two-body potential with large $a_s(0)$ and large $V_p(0)$, respectively. The dashed lines show the results predicted by our zero-range model that accounts for the spin-orbit coupling induced energy shifts. This model provides an excellent description of the numerical results for the Lennard-Jones potential, provided the length $(k_{\rm so})^{-1}$ associated with the spin-orbit coupling term is not too small compared to the van der Waals length $r_{\rm vdW}$, where $r_{\rm vdW}$ is given by $(2\mu C_6/\hbar^2)^{1/4}$ (in Figs. 1 and 2, the largest $k_{\rm so}r_{\rm vdW}$ considered corresponds to 0.4913 and 0.4171, respectively).

The dash-dotted lines in Figs. 1 and 2 show σ_{22} and K_{22} for the zero-range model when we set the spin-orbit coupling induced energy shifts artificially to zero. In this

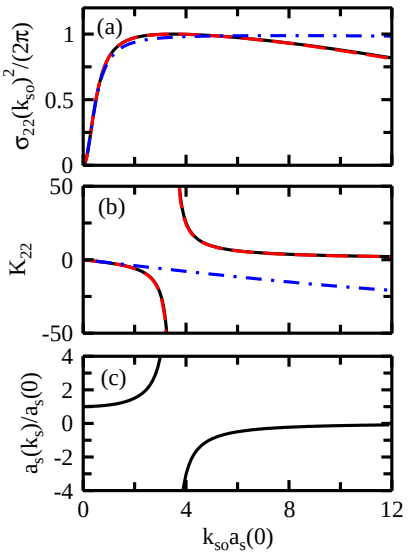

FIG. 1: (Color online) Large $a_s(0)$ case. The black solid line shows (a) the scaled partial cross section $\sigma_{22}(k_{\rm so})^2/(2\pi)$ and (b) the K-matrix element K_{22} for $E=0$ as a function of $k_{\rm so}a_s(0)$ for the Lennard-Jones potential with $a_s(0)/r_{\rm vdW} = 24.42$ and $V_p(0)/(r_{\rm vdW})^3 = -0.2380$ (this potential supports two s-wave bound states in free space). The red dashed line shows the result for the zero-range model developed in this work [see Eq. (11)]; the numerical results for the Lennard-Jones potential and the model are indistinguishable on the scale shown. To illustrate the importance of the energy shifts, the blue dash-dotted line shows the results for the zero-range model that artificially neglects the energy shifts. The solid line in (c) shows the scaled energy-dependent s-wave scattering length $a_s(k_s)/a_s(0)$, where $\hbar^2k_s^2 = 6\mu E_{\rm so}$.

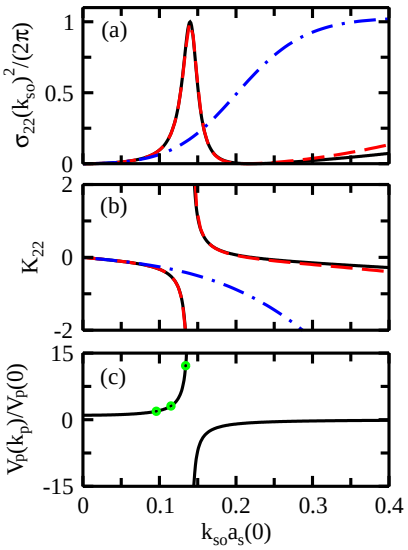

FIG. 2: (Color online) Large $V_p(0)$ case. The black solid line shows (a) the scaled partial cross section $\sigma_{22}(k_{\rm so})^2/(2\pi)$ and (b) the K-matrix element K_{22} for $E = 0$ as a function of $k_{\rm so}a_s(0)$ for the Lennard-Jones potential with $a_s(0)/r_{\rm vdW} = 0.9591$ and $V_p(0)/(r_{\rm vdW})^3 = 26.61$, corresponding to $a_s(0)/(V_p(0))^{1/3} = 0.3213$ (this potential supports 4 four s-wave bound states in free space). The red dashed line shows the result for the zero-range model developed in this work [see Eq. (11)]; the model reproduces the numerical results excellently for $k_{\rm so}a_s(0) \lesssim 0.3$. The blue dash-dotted line shows the results for the zero-range model that artificially neglects the energy shifts. The solid line in (c) shows the scaled energy-dependent p-wave scattering volume $V_p(k_p)/V_p(0)$, where $\hbar^2k_p^2 = -2\mu E_{\rm so}$. The green circles mark three of the four $k_{\rm so}a_s(0)$ values considered in Fig. 4.

case, the divergence in the K_{22} matrix element at finite $k_{\rm so}$ is not reproduced. For large $a_s(0)$ [see Fig. 1(a)], the model without energy shifts introduces deviations at the few percent level in the cross section σ_{22}. For large $V_p(0)$ [see Fig. 2(a)], in contrast, the model without the energy shifts provides a quantitatively and qualitatively poor description of the cross section σ_{22} even for relatively small $k_{\rm so}$ ($k_{\rm so}a_s(0) \gtrsim 0.05$). Figures 1(c) and 2(c) demonstrate that the divergence of the K_{22} matrix element occurs when the free-space scattering length $a_s(k_s)$, calculated at energy $3E_{\rm so}$, or the free-space scattering volume $V_p(k_p)$, calculated at energy $-E_{\rm so}$, diverge. We find that this occurs roughly when $a_s(0)k_{\rm so} \approx 10$ and $(V_p(0))^{1/3}k_{\rm so} \approx 0.21$; we checked that this holds quite generally, i.e., not only for the parameters considered in the figures. In Figs. 1(c) and 2(c), the "critical" $k_{\rm so}$ values correspond to $k_{\rm so}r_{\rm vdW} = 0.1423$ and $k_{\rm so}r_{\rm vdW} = 0.1462$, respectively. For comparison, using the $k_{\rm so}$ value for the one-dimensional realization of Ref. [4] and assuming $r_{\rm vdW} = 100a_0$, one finds $k_{\rm so}r_{\rm vdW} \approx 0.03$. This suggests that the phenomena discussed in the context of Figs. 1 and 2 should be relevant to future realizations of three-dimensional isotropic spin-orbit coupling experiments.

To further explore the two-particle scattering properties in the presence of spin-orbit coupling for short-range potentials with large free-space scattering volume $V_p(0)$, Figs. 3(a) and 3(b) show the partial cross section σ_{22} as a function of the scattering energy $-E_{\rm so} \leq E \leq 0$ and $0 \leq 0 \leq 400E_{\rm so}$, respectively, for $a_s(0)/(V_p(0))^{1/3} = 0.3213$ and $a_s(0)k_{\rm so} = 0.07673$. The results for the Lennard-Jones potential (dashed line) and square-well potential (solid line) are essentially indistinguishable on the scale shown. To assess the accuracy of our zero-range model, we focus on the Lennard-Jones potential and compare the numerically determined partial cross section $(\sigma_{22})^{\rm exact}$ with the partial cross section $(\sigma_{22})^{\rm zr}$ predicted using Eq. (11). Solid lines in Figs. 3(c) and 3(d) show the normalized difference Δ, defined through $\Delta = |(\sigma_{22})^{\rm zr} - (\sigma_{22})^{\rm exact}|/(\sigma_{22})^{\rm exact}$. The deviations are smaller than 1.3% for the scattering energies considered. Neglecting the spin-orbit coupling induced energy shifts in our zero-range model and calculating the normalized difference, we obtain the dashed lines in Figs. 3(c) and 3(d). Clearly, the zero-range model provides a faith-

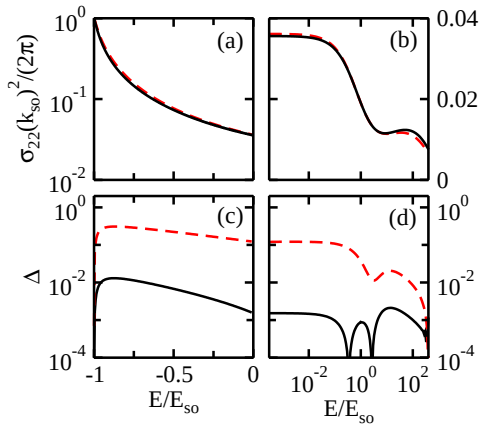

FIG. 3: (Color online) Large $V_p(0)$ case. (a) and (b): The red dashed and black solid lines show the scaled partial cross section $\sigma_{22}(k_{\rm so})^2/(2\pi)$ for the Lennard-Jones and square-well potential, respectively, as a function of the scattering energy E. For both potentials, we have $a_s(0)/(V_p(0))^{1/3} = 0.3213$ [$V_p(0) > 0$] and $k_{\rm so}a_s(0) = 0.07673$. The length scale associated with the spin-orbit coupling is notably larger than the range of the potential ($k_{\rm so}r_{\rm vdW} = 0.08$ for the Lennard-Jones potential and $k_{\rm so}r_{\rm sw} = 0.07676$ for the square-well potential). (c) and (d): The solid and dashed lines show the normalized difference Δ (see text) between the cross section for the Lennard-Jones potential and the zero-range model, obtained using Eq. (11), and between that for the Lennard-Jones potential and the zero-range model that neglects the spin-orbit coupling induced energy shifts, respectively. The zero-range model derived in this work (solid line) provides an excellent description (the deviations are smaller than 1.3 % for the data shown) over the entire energy regime. Panels (a) and (c) cover negative E (linear scale) while panels (b) and (d) cover positive E (logarithmic scale)].

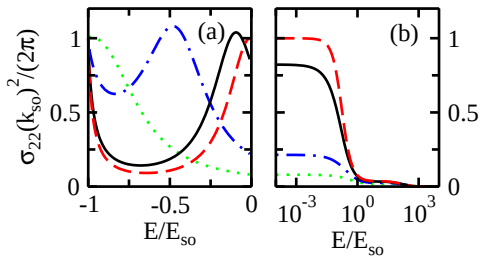

FIG. 4: (Color online) Scaled partial cross section $\sigma_{22}(k_{\rm so})^2/(2\pi)$ for the Lennard-Jones potential with $a_s(0)/(V_p(0))^{1/3} = 0.3213$ ($V_p(0) > 0$) and $a_s(0)/r_{\rm vdW} = 0.9591$ for four different $k_{\rm so}$ [the green dotted, blue dash-dotted, black solid, and red dashed lines correspond to $k_{\rm so}r_{\rm vdW} = 0.1$, $k_{\rm so}r_{\rm vdW} = 0.12$, $k_{\rm so}r_{\rm vdW} = 0.14$, and $k_{\rm so}r_{\rm vdW} = 0.146$, respectively] as a function of the scattering energy E [panel (a) covers negative E (linear scale) while panel (b) covers positive E (logarithmic scale)].

ful description of the full coupled-channels data for the Lennard-Jones potential only if the spin-orbit coupling induced energy shifts are included.

Figure 4 demonstrates that the non-quadratic single-particle dispersion relations have a profound impact on the low-energy scattering observables for a large free-space scattering volume. Specifically, the lines in Fig. 4 show the numerically obtained partial cross section σ_{22} as a function of the scattering energy for the same Lennard-Jones potential as that used in Figs. 2 and 3 for four different spin-orbit coupling strengths, namely $k_{\rm so}r_{\rm vdW} = 0.1$, 0.12, 0.14 and 0.146 [Fig. 3 used $k_{\rm so}r_{\rm vdW} = 0.08$; three of the four $k_{\rm so}$ values considered in Fig. 4 are marked by circles in Fig. 2(c)]. Figure 4 shows that the partial cross section depends sensitively on the spin-orbit coupling strength $k_{\rm so}$. This can be understood by realizing that a change in the spin-orbit coupling strength leads to a significant change of the $k_{\rm so}$-dependent scattering volume $V_p(k_p)$.

This paper revisited two-body scattering in the presence of single-particle interaction terms that lead, in the absence of two-body interactions, to non-quadratic dispersion relations. Restricting ourselves to three-dimensional isotropic spin-orbit coupling terms and spin-independent central two-body interactions, we developed an analytical coupled-channels theory that connects the short- and large-distance eigenfunctions using a generalized frame transformation. A key, previously overlooked result of our treatment is that the gauge transformation that converts the short-distance Hamiltonian to the "usual form" (i.e., a form without linear momentum dependence) introduces channel-dependent energy shifts. These energy shifts were then shown to appreciably alter the low-energy scattering observables, especially in the regime where the free-space scattering volume is large. To illustrate this, the $(J, M_J) = (0, 0)$ channel was considered exemplarily. Our framework provides the first complete analytical description that consistently accounts for all partial wave channels. Moreover, the first numerical coupled-channels results for two-particle Hamiltonian with realistic Lennard-Jones potentials in the presence of spin-orbit coupling terms were presented. The influence of the revised zero-range formulation put forward in this paper on two- and few-body bound states and on mean-field and beyond mean-field studies will be the topic of future publications.

I. ACKNOWLEDGEMENT

Support by the National Science Foundation through grant number PHY-1509892 is gratefully acknowledged. The authors acknowledge hospitality of and support (National Science Foundation under Grant No. NSF PHY-1125915) by the KITP. We thank J. Jacob for providing us with a copy of his coupled-channels code.

[1] C. Chin, R. Grimm, P. Julienne, and E. Tiesinga, Feshbach resonances in ultracold gases, Rev. Mod. Phys. **82**, 1225 (2010).

[2] I. Bloch, J. Dalibard, and W. Zwerger, Many-body physics with ultracold gases, Rev. Mod. Phys. **80**, 885 (2008).

[3] Theory of ultracold atomic Fermi gases, S. Giorgini, L. P. Pitaevskii, and S. Stringari, Rev. Mod. Phys. **80**, 1215 (2008).

[4] Y.-J. Lin, K. Jiménez-García, and I. B. Spielman, Spin-orbit-coupled Bose-Einstein condensates, Nature (London) **471**, 83 (2011).

[5] J. Dalibard, F. Gerbier, G. Juzeliūnas, and P. Öhberg, Colloquium: Artificial gauge potentials for neutral atoms, Rev. Mod. Phys. **83**, 1523 (2011).

[6] V. Galitski and I. B. Spielman, Spin-orbit coupling in quantum gases, Nature **494**, 49 (2013).

[7] H. Zhai, Degenerate quantum gases with spin-orbit coupling: a review, Rep. Prog. Phys. **78**, 026001 (2015).

[8] H. Zhai, Spin-Orbit Coupled Quantum Gases, Int. J. Mod. Phys. B **26**, 1230001 (2012).

[9] X. Cui, Mixed-partial-wave scattering with spin-orbit coupling and validity of pseudopotentials, Phys. Rev. A **85**, 022705 (2012).

[10] P. Zhang, L. Zhang, and Y. Deng, Modified Bethe-Peierls boundary condition for ultracold atoms with spin-orbit coupling, Phys. Rev. A **86**, 053608 (2012).

[11] Z. Yu, Short-range correlations in dilute atomic Fermi gases with spin-orbit coupling, Phys. Rev. A **85**, 042711 (2012).

[12] L. Zhang, Y. Deng, and P. Zhang, Scattering and effective interactions of ultracold atoms with spin-orbit coupling, Phys. Rev. A **87**, 053626 (2013).

[13] H. Duan, L. You, and B. Gao, Ultracold collisions in the presence of synthetic spin-orbit coupling, Phys. Rev. A **87**, 052708 (2013).

[14] Y. -C. Zhang, S. -W. Song, W. -M. Liu, The confinement induced resonance in spin-orbit coupled cold atoms with Raman coupling, Sci. Rep. **4**, 4992 (2014).

[15] S.-J. Wang and C. H. Greene, General formalism for ultracold scattering with isotropic spin-orbit coupling, Phys. Rev. A **91**, 022706 (2015).

[16] Q. Guan and D. Blume, Scattering framework for two particles with isotropic spin-orbit coupling applicable to all energies, Phys. Rev. A **94**, 022706 (2016).

[17] Y. Wu and Z. Yu, Short-range asymptotic behavior of the wave functions of interacting spin-1/2 fermionic atoms with spin-orbit coupling: A model study, Phys. Rev. A **87**, 032703 (2013).

[18] D. Blume and C. H. Greene, Fermi pseudopotential approximation: Two particles under external confinement, Phys. Rev. A **65**, 043613 (2002).

[19] E. L. Bolda, E. Tiesinga, and P. S. Julienne, Effective-scattering-length model of ultracold atomic collisions and Feshbach resonances in tight harmonic traps, Phys. Rev. A **66**, 013403 (2002).

[20] Here and in what follows, underlined quantities are matrices.

[21] U. Fano, Stark effect of nonhydrogenic Rydberg spectra, Phys. Rev. A **24**, 619(R), (1981).

[22] D. A. Harmin, Theory of the Nonhydrogenic Stark Effect, Phys. Rev. Lett. **49**, 128 (1982).

[23] C. H. Greene, Negative-ion photodetachment in a weak magnetic field, Phys. Rev. A **36**, 4236 (1987).

[24] B. E. Granger and D. Blume, Tuning the Interactions of Spin-Polarized Fermions Using Quasi-One-Dimensional Confinement, Phys. Rev. Lett. **92**, 133202 (2004).

[25] S.-J. Wang, Ph.D thesis, Purdue University (2016).

[26] B. R. Johnson, The Multichannel Log-Derivative Method for Scattering Calculations, J. Comput. Phys. **13**, 445 (1973).

[27] F. Mrugała and D. Secrest, The generalized log-derivative method for inelastic and reactive collisions, J. Chem. Phys. **78**, 5954 (1983).